



Heat transfer and pressure drop characteristics of MgO nanofluid in a double pipe heat exchanger

H. Arya¹ · M. M. Sarafraz² · O. Pourmehran² · M. Arjomandi²

Received: 24 February 2018 / Accepted: 15 December 2018 / Published online: 4 January 2019
© Springer-Verlag GmbH Germany, part of Springer Nature 2019

Abstract

The present work aims to investigate the plausible application of MgO-ethylene glycol as a heat transfer fluid in a double-pipe heat exchanger. The nanofluid was prepared using a two-step method at weight concentrations of 0.1, 0.2 and 0.3%. The test rig provided conditions to measure the convective heat transfer coefficient, pressure drop and friction factor of the system. Influence of the different operating parameters such as flow rate, mass concentration of nanoparticles and inlet temperature of nanofluid to the heat exchanger on the heat transfer coefficient and pressure drop was experimentally investigated. Results showed that the heat transfer coefficient within the heat exchanger can be enhanced by 27% for wt.% = 0.3 in comparison with the base fluid (ethylene glycol). It was also found that the presence of MgO nanoparticles increased the pressure drop by 35% at wt.% = 0.3. The friction factor of the system decreased nonlinearly with an increase in the Reynold number and it followed the trend of 64/Re equation. An increase in the mass concentration of nanoparticles increased the friction factor and the maximum friction factor enhancement was 32% belonging to the nanofluid with mass concentration of wt.% = 0.3. Likewise, inlet temperature was found to have a very slight influence on the heat transfer coefficient and no effect on the friction factor and pressure drop of the system. The thermo-physical properties of MgO-ethylene glycol nanofluid was also experimentally measured at various temperatures.

Nomenclature

A	Area, m ²
C _p	Heat capacity, J.kg ⁻¹ .°C ⁻¹
<i>f</i>	Fanning friction factor
<i>h</i>	Convective heat transfer coefficient, W.m ⁻² . K ⁻¹
<i>k</i>	Thermal conductivity, W.m ⁻¹ .°C ⁻¹
<i>L</i>	Length, m
Nu	Nusselt number
<i>P</i>	Pressure, Pa
<i>Q</i>	Heat, W
Re	Reynolds number
<i>T</i>	Temperature, °C
<i>U</i>	Heat transfer coefficient, W. m ⁻² . K ⁻¹
wt.%	Weight fraction

bs	Base fluid
hot	Heating loop
nf	Nano-fluid
cold	Cooling loop
<i>in</i>	Inlet
<i>out</i>	Outlet
<i>m</i>	Mean
<i>m</i>	Mass flow, kg.s ⁻¹
<i>w</i>	Wall

Greek symbols

Δ	Difference
---	------------

Subscripts-superscripts

ave	Average
b	Bulk

✉ M. M. Sarafraz
mohamadmohsensarafraz@gmail.com

¹ Centre for Energy Resource Engineering, Technical University of Denmark, Kongens Lyngby, Denmark

² School of Mechanical Engineering, The University of Adelaide, Adelaide, South Australia, Australia

1 Introduction

Heat exchangers play a key role in various industries including (but not limited to) food, brewery and oil and petrochemical industries in which cooling and/or heating a working fluid is required. A heat exchanger provides sufficient contact area for one, two or more working fluids to exchange the significant amount of heat in a confined space. Thereby, different types of heat exchangers are currently utilised in the industrial sector depending on the required thermal specifications and the heat transfer demands [1, 2]. Plate heat exchanger is one of the efficient and common used type of heat exchangers,

providing great specific surface area and anomalous heat transfer coefficient. However, recent investigations have shown that this type of heat exchangers suffers from the limitation of size, pressure drop and limited operating temperature. Therefore, much effort has been made to enhance the thermal performance of the heat exchangers using active and passive techniques. One plausible technique to increase the thermal performance of a heat exchanger is to use the extended surfaces such as pins or fins to increase the surface area. This results in the better heat transport from the walls of the heat exchanger to the fluid, however, this also intensifies the pressure drop within the heat exchanger [3–5].

One other potential solution to enhance the heat exchanger thermal performance is to use the working fluids with improved thermal features. Nanofluid is a colloidal mixture of conductive solid particles dispersed within a conventional coolant such as water, oil or ethylene glycol. The mean size of the nanoparticles is less than 100 nm and the uniform dispersion of the nanoparticles enhances the thermo-physical properties of the base fluid such as thermal conductivity and heat capacity. Since Choi [6] introduced the application of nanofluid in the cooling systems, much effort has been made to broaden the application of the nanofluids to in different thermal engineering systems. In some studies, it has been shown that the presence of nanoparticles within the base fluid results in the plausible enhancement in the thermal conductivity and density of nanofluid. However, disadvantage of presence of nanoparticles is reflected in the increase in the pressure drop and decrease in the heat capacity. Also, the instability of the nanofluid is another challenge associated with the preparation and the production of the nanofluids. In an unstable nanofluid, nanoparticles deposit on the bottom of the container. Hence, the thermo-physical properties of nanofluid is not constant over the time, which adds uncertainty to the performance of the nanofluids.

There are also other studies, which focus on the single-phase and two-phase flow heat transfer characteristics of the nanofluids in different heat exchanging media. For example, Han et al. [7] conducted a set of experiments to assess the influence of alumina aqueous nanofluid on the heat transfer enhancement inside a double pipe heat exchanger at different bulk temperatures. Nanofluids were prepared at volumetric concentration of 0.25 and 0.5%. Results showed that the heat transfer increases with the increase in temperature and volume concentration of nano-particles. For the case of nanofluid, significant improvement in thermal performance of the system was observed in comparison with water with maximum Nusselt number increase up to 24.5% at 50 °C (inlet temperature). In another study conducted by Bahraei et al. [8], thermal and hydraulic characteristics of a non-Newtonian hybrid nanofluid were investigated in a double-tube mini-channel heat exchanger. They used two nanofluids namely Tetra Methyl Ammonium Hydroxide (TMAH) coated Fe_3O_4

nanoparticles and Gum Arabic (GA) coated Carbon Nanotubes (CNTs). Variable thermal conductivity and viscosity were applied in the simulations. The results showed that the addition of nanoparticles causes a further increment in heat transfer rate at lower Reynolds numbers, such that the increase in heat transfer rate of the nanofluid (in comparison with water) at Reynolds numbers 500 and 2000 is 53.8 and 28.6%, respectively. Kabeel et al. [9] designed and fabricated an experimental loop to investigate the heat transfer characteristics and pressure drop for corrugated plate heat exchange. The plate geometry and hydraulic characteristics is cleared in their literature. The experiments were carried out under various concentration of nanofluid (vol.% = 1–4). They demonstrated that, both the heat transfer and the pumping power were increased with the nanofluid concentrations. The heat transfer coefficient was increased by 13 at 4% nano fluid concentrations. The uncertainties for their experiments were 9.8%.

Thermo-hydraulic performance of the heat exchanger has also been targeted in many studies. For instance, numerical and experimental study were conducted by Sarkar et al. [10] to assess the thermo-hydraulic performance of a plate heat exchanger working with a hybrid nanofluid (alumina + multi walled carbon nanotube) dispersed in water and to investigate the effect of nanofluid on the heat transfer and pressure drop. Influence of different operating parameters such as inlet temperature, flow rate and volume concentration of nanoparticles were studied. It was found that by using hybrid nanofluid, the heat transfer coefficient was enhanced by 39.1% with negligible increase in pumping power of 1.2% (reduction). Tiwari et al. [11] conducted a set of experiments to investigate a chevron-type corrugated plate heat exchanger heat transfer characteristics and pressure drop when using CeO_2 /water nanofluid. The optimum nanoparticle concentration that leads to maximum heat transfer coefficient was determined. A maximum heat transfer enhancement of 39% at vol.% = 0.75 was achieved. The study also showed the enhancement in heat transfer coefficient when the nanofluid temperature was decreased, which was against the results published in the literature [12].

In a work conducted by Vinod et al. [13], three different non-Newtonian nanofluids were prepared from the dispersion of Fe_2O_3 , Al_2O_3 and CuO nanoparticles in an aqueous carboxymethyl cellulose (CMC) base fluid. They used a shell and helical coil heat exchanger to conduct some experiments on nanofluids. The nanofluids were prepared at weight concentration of 0.2–1.0%. Nanofluid and water were used on shell side and tube side, respectively. The results showed that the Nusselt number increased with an increase in the concentration of nanofluid, temperature of flow in the shell side, Dean number (flow rate of coil-side water), and stirrer speeds. It was found that the CuO/CMC-based nanofluid has better heat transfer than the other two types of nanofluid. The heat transfer performance of nanofluids was significantly enhanced

at higher nanofluid concentrations, shell-side temperatures, stirrer speeds and Dean numbers.

Kumar et al. [14] investigated the characterization, heat transfer and exergetic performance of a nanofluid in a plate heat exchanger (PHE). They employed two types of nanofluids namely $\text{CeO}_2/\text{water}$ and ZnO/water . The experimental outcomes were compared to water and the nanofluids at various concentrations. Results revealed that the best heat transfer performance can be obtained with ZnO/water nanofluid. The volume concentration of the nanofluids varied from 0.5 to 2.0% (volumetric concentration). The Flow rate of the coolant varied from 0.5.0 to 2.0 lpm and the flow rate of the hot fluid was 2 lpm. The inlet temperatures of cold and hot fluid were 25 and 50 °C respectively.

In contrast to the above literature, in some studies, the presence of nanoparticles resulted in a decrease in the thermal performance of the system. For example, in a study conducted by Zhang et al. [15], the graphene oxide-water nanofluid at wt.% = 0 to 0.05% was tested in a high heat flux heat exchanger and it was found that the thermal performance of the system with nanofluid in two-phase and single-phase regions (near the onset of boiling) is deteriorated. The main reason for the reduction in heat transfer coefficient was attributed to the deposition of the nanoparticles and instability of the nanofluid. The same trend was also found in natural convection and pool boiling heat transfer of alumina-water nanofluid conducted by Das et al. [16]. The experiments were carried out at vol.% = 1 to 4% of alumina nanoparticles dispersed in water. The deterioration was seen both in convective and boiling heat transfer region. Anoop et al. [17] also investigated the thermal performance of the nanofluids in some industrial heat exchangers at three mass particle concentrations of 2, 4, and 6% of silicon dioxide–water nanofluids. Experiments were conducted to assess the average heat transfer coefficient and the pressure drop of water as a base fluid versus nanofluid. Experimental results demonstrated the augmentation of the pressure drop and also a significant deterioration of heat transfer coefficient for nanofluids through the heat exchangers. Likewise, the measured pressure drop for nanofluids showed an increase in the pressure drop in comparison with that of measured for the water. They concluded that this enhancement can limit the application of nanofluid in industrial systems.

Faced with the above literature review, following gap was identified:

Despite extensive research conducted on the application of nanofluid in heat exchangers, the outcomes are still controversial. Some studies have shown a reduction in the heat transfer due to the presence of the nanoparticles and their thermal resistance, while some studies revealed the positive influence of using nanofluid in the heat exchanger due to the enhancement in thermo-physical properties of the base fluid. There are also controversial reports on the role of inlet temperature of nanofluid on the overall performance of heat exchanger.

Hence, more studies are required to develop better insight on the plausible application of nanofluid and the mechanisms involved in the heat transfer systems. Hence, in the present study, Magnesium oxide (MgO) nanoparticles is targeted as in our preliminary assessments, it has shown some plausible thermal features and can be a promising working fluid for the thermal engineering systems. Thus, in the present work, an experimental investigation has been conducted to understand the influence of different operating parameters including the inlet temperature, the flow rate and the mass concentration of the nanofluid on the average heat transfer coefficient, friction factor and the pressure drop of the heat exchanger. Also, the thermo-physical properties of the nanofluid are experimentally measured, which can be helpful for justifying the outcomes of the experiments.

2 Experimental

2.1 Test rig

Figure 1 presents a schematic diagram of the experimental test rig used for the present research. The rig consists of three main units including (1) nanofluid hot loop, (2) water cooling loop, (3) measurement instruments including pressure sensors, an ultrasonic flow meter, and thermocouples, which all were connected to a data logger. Nanofluid was loaded into the nanofluid tank and circulated inside the hot loop using a centrifugal DAB pump (model HT, maximum flow rate 20 l/min). The same pump was also employed to circulate water in the cooling loop. Hot loop was passed through the tube and the cooling water was circulated within the annulus. To maintain the required flow rate, a bypass cycle was in place to control the rate of the flow. Notably, the flow rate of both loops was controlled with an ultrasonic flow meter (0–50 l/min, accuracy: 0.1% of reading fabricated by Flownetix). The pressure and temperature of the nanofluid were measured before and after the test section using pressure transmitter and k-type thermocouples (both manufactured by Omega with accuracy of 1% of reading and 0.1 K, respectively). Likewise, eight different k-type thermocouples were mounted on different axial locations of the test heat exchanger to measure the wall temperature of the heat exchanger at different locations of the inner tube to obtain the axial wall temperature profile within the tube side of the heat exchanger. The distance between the thermocouples was 20 cm as represented in Fig. 1.

The test heat exchanger was a cooper-made double pipe heat exchanger with inner and outer diameters (ID and OD) of 6.35 and 12.7 mm respectively (in accordance with ANSI/ASME/API 5 L) and the tube length of 230 cm. Notably, the distance between k-type thermocouples was 20 cm and the distance from the inlet port to the first thermocouple was 30 cm. Also, the distance between the last

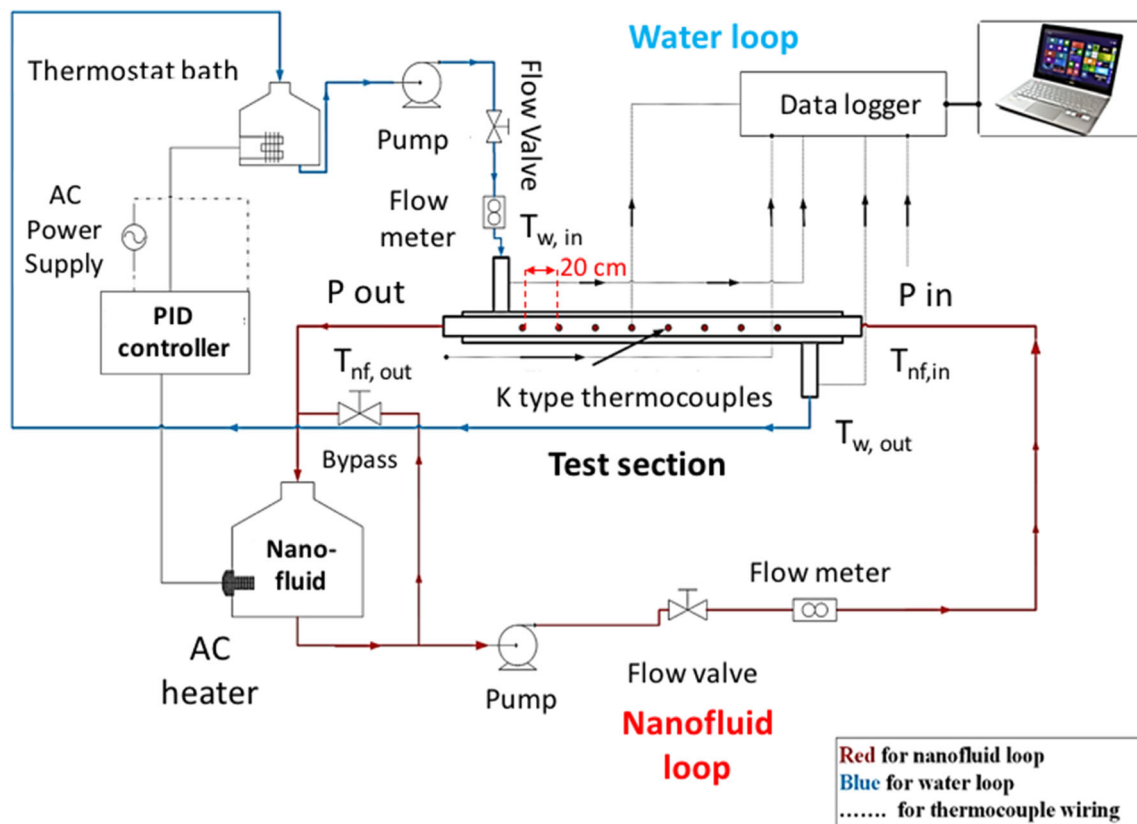


Fig. 1 A schematic diagram of the experimental test rig used in the present research

thermocouple and the outlet port was 30 cm as well. Since k-type ones were mounted on the wall of the tube, they had no influence on each other and they did not induce any agitation or perturbation in the fluid flow. Silicone paste with thermal conductivity of 5 W/m. K was injected in the thermo-wells to minimise the contact thermal resistance between the thermocouples and the wall of the tube. The reading values from the pressure sensor, thermocouples and flow meter were directly collected with a data logger fabricated by National Instruments (NI) with frequency of 1 kHz. Noticeably, the temperature of the nanofluid tank was kept constant using a thermostat bath and an auxiliary heater. A PID controller maintained the temperature of the tank. The experiments were conducted three times to ensure about the repeatability and predictability of the results and the obtained results were within the deviation of $\pm 2.1\%$.

2.2 Preparation of nanofluid and characterization

To prepare the nanofluid, a two-step method was employed. MgO nanoparticles were used as a solid conductive material and ethylene glycol (EG) was used as the base fluid. The nanoparticles were dispersed into the ethylene glycol using the following simple procedure:

- The desired weight of the nanoparticles was measured using a mass balancer. The desired mass of the ethylene glycol was also measured (basis: 1 kg).
- The MgO nanoparticles were added into the ethylene glycol and a magnetic stirrer was used to disperse the nanoparticles into the ethylene glycol. Nonyl phenol ethoxilate was used at $\text{vol.}\% = 0.1$ of general volume of nanofluid to decrease the agglomeration and to increase the stability of the nanofluid following our previous works [18, 19].

The ultrasonic homogenizer was used to crack the agglomeration of the nanoparticles within the base fluid and to uniformly disperse the nanoparticles. Notably, the nanofluids were prepared at $\text{wt.}\% = 0.1, 0.2\%$ and 0.3% . Notably, the experiments were conducted only at $\text{wt.}\% = 0.1\text{--}0.3\%$ of MgO in ethylene glycol. This is because, the stability of the nanofluid could not be secured. Not only the amount of agglomeration and clustering, but also the gravitational sedimentation of nanoparticles increased at $\text{wt.}\% > 0.3$. Hence, the experiments were conducted within the range of $\text{wt.}\% = 0.1$ to 0.3% .

To perform the characterization, scanning and transmission electron microscopic images were taken from the MgO nanoparticles and MgO-ethylene glycol nanofluid to analyse the morphology and particle size of the

nanoparticle. Figure 2a shows the morphology and size of the nanoparticles. As can be seen, nanoparticles are identical in terms of size and morphology. The morphology is spherical and the nanoparticles are uniform in terms of size. To confirm the size of nanoparticle, the particle size count test was performed using digital scattering light device (zeta sizer) as represented in Fig. 2b. As can be seen, the dominant size of the nanoparticles is 50 nm, which is in accordance with the results obtained with the scanning electron microscopic image. Figure 2c shows the transmission electron microscopic (TEM) image for the dispersion of nanoparticles in ethylene glycol. As can be seen, the nanoparticles have been dispersed within the base fluid despite several agglomerated spots, which are formed due to the attraction forces between the nanoparticles. It also shows that the nanoparticles have been dispersed uniformly within the base fluid. Also, the TEM image further confirmed the size of the nanoparticles.

2.3 Data reduction and uncertainty analysis

For the hot loop, the heat transfer can be estimated using following correlations:

$$Q_{nf}^{hot} = m_{nf} \cdot C_{p,nf} (T_{in,nf} - T_{out,nf}) \quad (1)$$

For the cooling loop, rate of heat transfer can be calculated by the following correlation:

$$Q_w^{cold} = m_w \cdot C_{p,w} (T_{in,w} - T_{out,w}) \quad (2)$$

In Eq. (1), Q_{nf}^{hot} is the rate of heat transfer belonging to hot nano-fluid, m_{nf} is quantity of mass flow the hot nano-fluid. In Eq. (2), Q_w^{cold} is the rate of heat transfer belonging to cooling loop and m_w is quantity of mass flow of water. The average heat transfer rate is defined as follows:

$$Q_{ave} = \frac{Q_{nf}^{hot} + Q_w^{cold}}{2} \quad (3)$$

where, Q_{ave} is the arithmetic average of heat transfer rate between the heating and cooling loops. To calculate the heat transfer coefficient of nano-fluid, u , following equation is utilized as:

$$U_{nf} = \frac{Q_{ave}}{T_w - T_{b,nf}} \quad (4)$$

In this equation, T_w is the arithmetic average of the reading values form eight thermocouples mounted on the wall of inner tube. T_b is the bulk temperature (film or caloric temperature) of nano-fluids, which can be calculated as the arithmetic average of inlet and outlet temperatures of the inner tube. Notably, the heat loss from the heat exchanger, tanks and pipes to the environment can influence the average heat transfer coefficient. However, the difference between the heat provided by the AC heater ($Q = V \cdot I$) to nanofluid (V and I are voltage and current applied to the heater) and the heat calculated by Eq. (1) is less than 5%. This is because all the pipes, joints and tanks were heavily insulated with glass wool. Nusselt and Reynolds numbers can also be calculated through Eqs. (5-6) respectively:

$$Nu_{nf} = \frac{h_{nf} \cdot D_i}{k_{nf}} \quad (5)$$

$$Re_{nf} = \frac{\rho_{nf} \cdot u_{nf} \cdot D_i}{\mu_{nf}} \quad (6)$$

The friction factor of the system was measured using the following correlations:

$$f = \frac{\Delta p}{\frac{l}{d} \times \frac{2 \times u^2}{\rho}} \quad (7)$$

Here, f is the friction factor, Δp is the pressure drop of the system, which is measured experimentally using two pressure transmitters installed before and after the inner tube, l is the length of the tube, d is the diameter of the tube side and u is the velocity of the working fluid which can be determined from the flow rate of the flow.

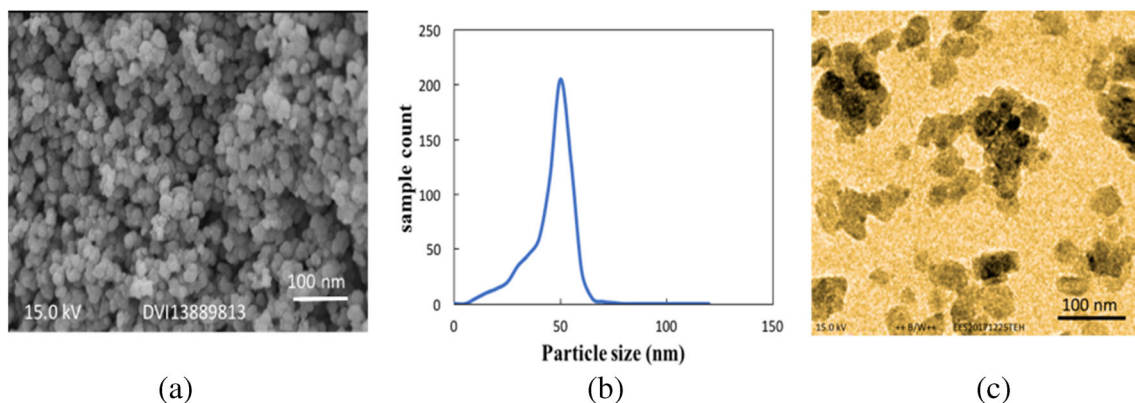


Fig. 2 Characterization of nanoparticles used in the present research

To evaluate the uncertainty of the experimental data, the sequential perturbation method introduced by Moffat was used following the works [20, 21]. According to this method and the uncertainty of the instruments, the total uncertainty of heat transfer coefficient is about 8.93%. The uncertainty for the pressure drop and friction factor were 6.2 and 6%, respectively. The uncertainty value for the Reynolds number and the Nusselt number was 5.9 and 9%, respectively. For validating the results, deionized water was tested inside the test rig. The obtained results were compared to the results obtained with the well-known correlations of Dittus-Boelter and Gnielinski [22] for the heat transfer coefficient and Colebrook [23] for the friction factor. Results of the comparison showed that the experimental data are in a good agreement with those of obtained by correlations with the deviation of 6.3, 5.4 and 7.9% against Gnielinski, Dittus-Boelter and Colebrook correlations, respectively. Figure 3a, b show the results of the calibration with deionized water for heat transfer coefficient and friction factor.

2.4 Physical properties of nanofluid

The viscosity of the nanofluids was measured using DV-II + PRO digital viscometers (manufactured by Brookfield CO., Accuracy: $\pm 1.0\%$ of reading/Repeatability: $\pm 0.2\%$). Density was measured using DMA 4500 ME (manufactured by Anton Paar Co., Accuracy: $\pm 1.0\%$ of reading/Repeatability: 0.00001 g/cm^3). Thermal conductivity was measured with DTC300 (manufactured by TA Instrument, Accuracy: $\pm 1\%$). Heat capacity was measured with DSC METTLER TOLEDO instrument (accuracy: $\pm 1\%$ reading). Figure 4 represents the dependence on temperature of thermo-physical properties of MgO-EG nanofluids at wt.% = 0.1 to 0.3 for temperature range of 25–100 °C. As can be seen, with an increase in the mass concentration of the nanofluid, density, viscosity and thermal conductivity of the nanofluid increase, while the heat capacity of the nanofluid decreases. This is because the

thermal conductivity, density and viscosity of MgO is relatively larger than water, thereby resulting in the enhancement of the thermal features of water. Interestingly, with an increase in the temperature, density changes very slightly, while thermal conductivity and heat capacity of the nanofluid increase. Also, the viscosity of the nanofluid decreases. Within the range of 25–60 °C in which the experiments were conducted, an increase in the thermal conductivity, heat capacity and density with temperature is very small (e.g. 0.1% for density and 0.4% for thermal conductivity at wt.% = 0.3). Hence, it can be expected that temperature has a very slight influence on the thermal performance of the nanofluid within the temperature range of 25–60 °C.

3 Results and discussion

3.1 Flow rate

Figure 5 presents the dependence of heat transfer coefficient on the Reynolds number at 50 °C and for different mass concentrations of nanofluid and also in comparison with the base fluid. As can be seen, with an increase in the flow rate of the nanofluid, higher heat transfer coefficient was achieved. For example, for nanofluid at wt.% = 0.1, at $Re = 1300$, the heat transfer coefficient is $2178 \text{ W/m}^2 \cdot \text{K}$, while at $Re = 9300$, the heat transfer coefficient is $6259 \text{ W/m}^2 \cdot \text{K}$. Noticeably, the heat transfer coefficient was higher in transient and turbulent region in comparison with the ones measured in the laminar flow, which is in accordance with the literature [24]. For example, in $Re = 600$ (the laminar regime), the heat transfer coefficient is $1584 \text{ W/m}^2 \cdot \text{K}$, while at $Re = 6500$, the heat transfer coefficient is $5467 \text{ W/m}^2 \cdot \text{K}$. This is because, an increase in the flow rate of the nanofluid, intensifies the movement of nanoparticles within the base fluid. Nanoparticles are energy carriers and absorb the thermal energy near the hot walls and

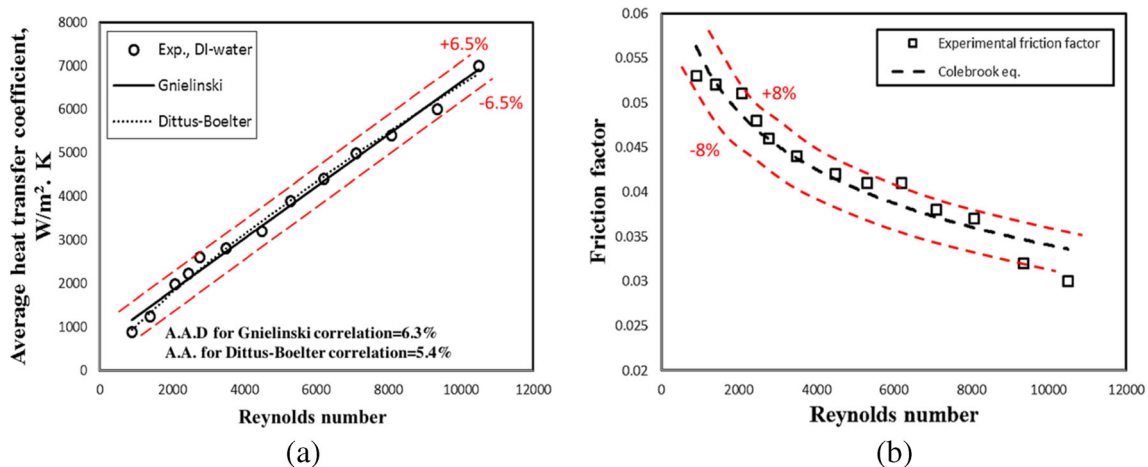


Fig. 3 a Results of the calibration and comparison between Dittus-Boelter and Gnielinski correlations against experimental data related to DI-water b Results of calibration belonging to friction factor in comparison with Colebrook equation

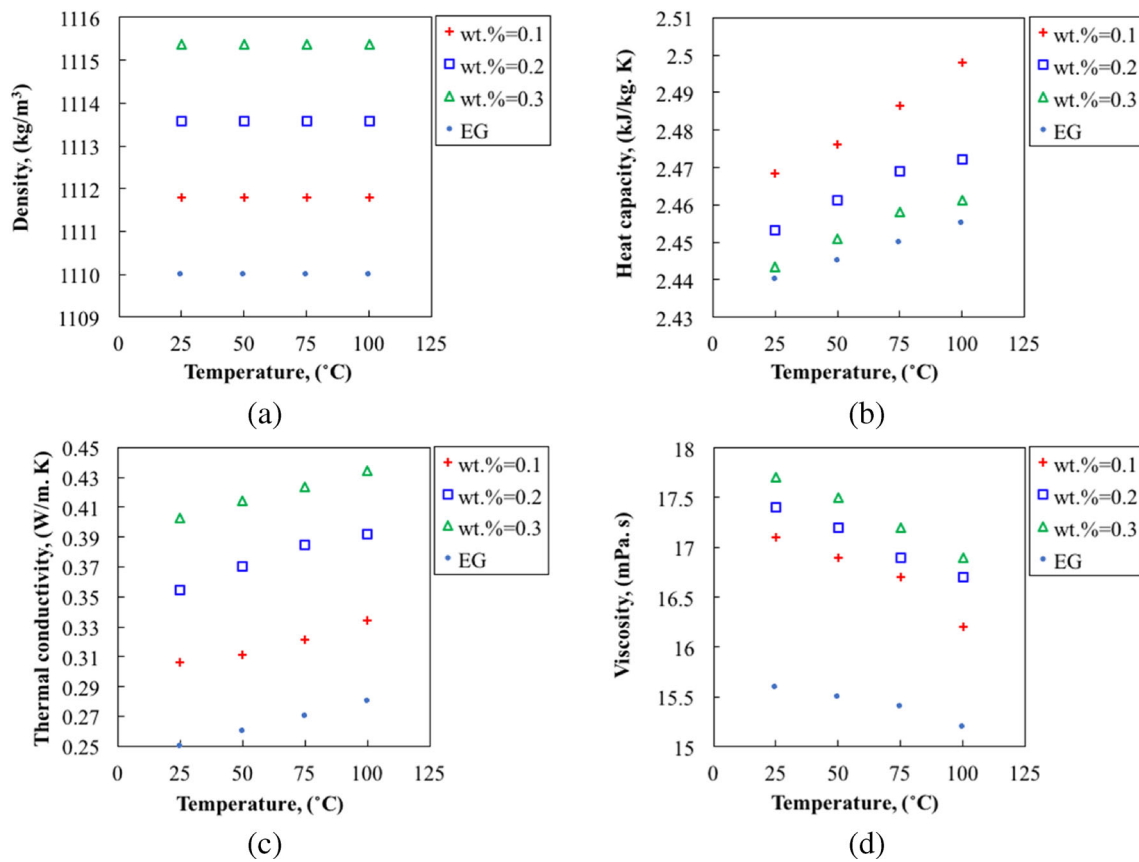


Fig. 4 The Dependence on temperature of the physical properties of MgO-EG nanofluids for various mass concentrations of MgO, **a** density versus temperature, **b** heat capacity versus temperature, **c** thermal conductivity versus temperature, **d** viscosity versus temperature

transport it to the cold part of the base fluid. Overall, the higher the flow rate is, the higher heat transfer can be achieved. The same trend is also seen for the Nusselt number. As can be seen in Fig. 6, the Nusselt number increases with an increase in the flow rate of flow. Importantly, the Nusselt number lies

between the range of 15 and 90, which is in accordance with the literature [25]. Also, for a given Reynolds number e.g. 10,100, the heat transfer coefficient at wt.% = 0.3 is 7607 W/m². K, while it is 5990 W/m². K for the base fluid and 6589 W/m². K for nanofluid at wt.% = 0.1. Hence, the

Fig. 5 Dependence of heat transfer coefficient on Reynolds number for different mass concentration of nanofluids

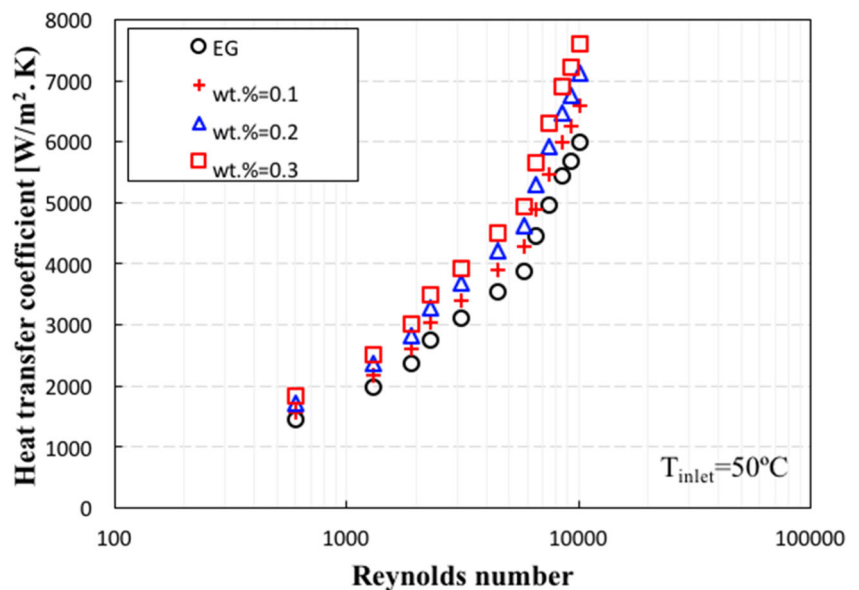
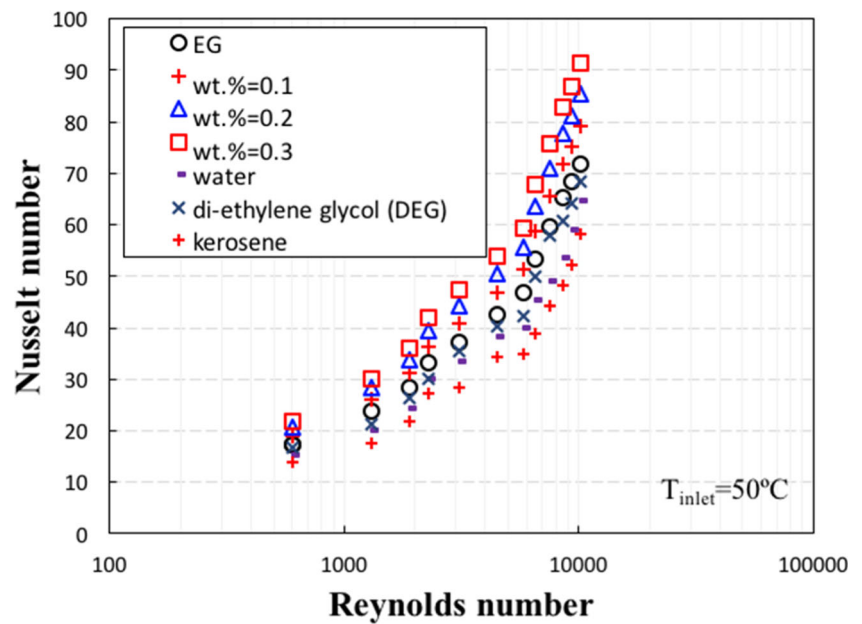


Fig. 6 Dependence of Nusselt number on Reynolds number for different mass concentration of nanofluids



presence of the nanoparticles intensifies the heat transfer coefficient of the heat exchanger. Figure 6 represents the dependence of the Nusselt number on the Reynolds number for various nanofluids and three conventional working fluids. As can be seen, the experimental Nusselt number for the nanofluids, regardless of the concentrations of the nanoparticles, was larger than that of measured for water, di-ethylene glycol (DEG), ethylene glycol and kerosene. This is because, the phenomena including Brownian motion and thermophoresis effect can intensify the convective heat transfer within the nanofluids. Hence, in a back-to-back comparison, nanofluids present better thermal performance in comparison with the conventional coolants. For example, the heat transfer coefficient measured for MgO/EG at wt.% = 0.3 and $Re = 10,100$ is 56% larger than

that of measured for kerosene and 33.5% larger than that of recorded for MEG.

3.2 Mass concentration of nanofluid

As already shown in Fig. 4, the presence of the nanoparticles within the base fluid changes the thermal properties of ethylene glycol. As represented in Fig. 5, with an increase in the mass concentration of nanofluid, higher heat transfer coefficient was achieved. For example, for a given Reynolds number such as Reynolds number of 4500, at wt.% = 0.1, the heat transfer coefficient is $3894 \text{ W/m}^2 \cdot \text{K}$, while it reaches $4495 \text{ W/m}^2 \cdot \text{K}$ at wt.% = 0.3. The reason for the enhancement of heat transfer coefficient is attributed to the enhancement in the

Fig. 7 Dependence of heat transfer coefficient on Reynolds number at different inlet temperatures of nanofluid at wt.% = 0.3

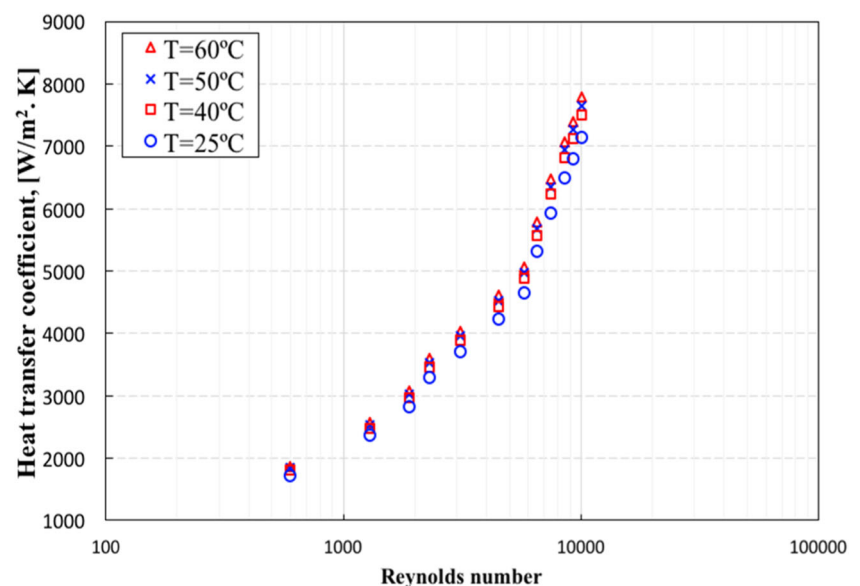


Table 1 Enhancement in heat transfer coefficient and thermal conductivity of nanofluid

Nanofluid	Enhancement in HTC	Enhancement in thermal conductivity
T = 40 °C		
wt.% = 0.1	2.9%	$k_{nf, T} / k_{nf, 25^\circ C} = 1.01$
wt.% = 0.2	4.4%	$k_{nf, T} / k_{nf, 25^\circ C} = 1.02$
wt.% = 0.3	8.6%	$k_{nf, T} / k_{nf, 25^\circ C} = 1.04$
T = 50 °C		
wt.% = 0.1	4.2%	$k_{nf, T} / k_{nf, 25^\circ C} = 1.02$
wt.% = 0.2	6.2%	$k_{nf, T} / k_{nf, 25^\circ C} = 1.04$
wt.% = 0.3	8.9%	$k_{nf, T} / k_{nf, 25^\circ C} = 1.05$
T = 60 °C		
wt.% = 0.1	6.3%	$k_{nf, T} / k_{nf, 25^\circ C} = 1.02$
wt.% = 0.2	8.1%	$k_{nf, T} / k_{nf, 25^\circ C} = 1.06$
wt.% = 0.3	9.7%	$k_{nf, T} / k_{nf, 25^\circ C} = 1.09$

Brownian motion of the nanoparticles within the base fluid. With an increase in the mass concentration of nanofluid, more nanoparticles are available within the base fluid and also adjacent to the wall of the heat exchanger. Thus, more collision and more random movements of particles are likely to occur resulting in better heat transport from a region with high temperature to the region with low temperature.

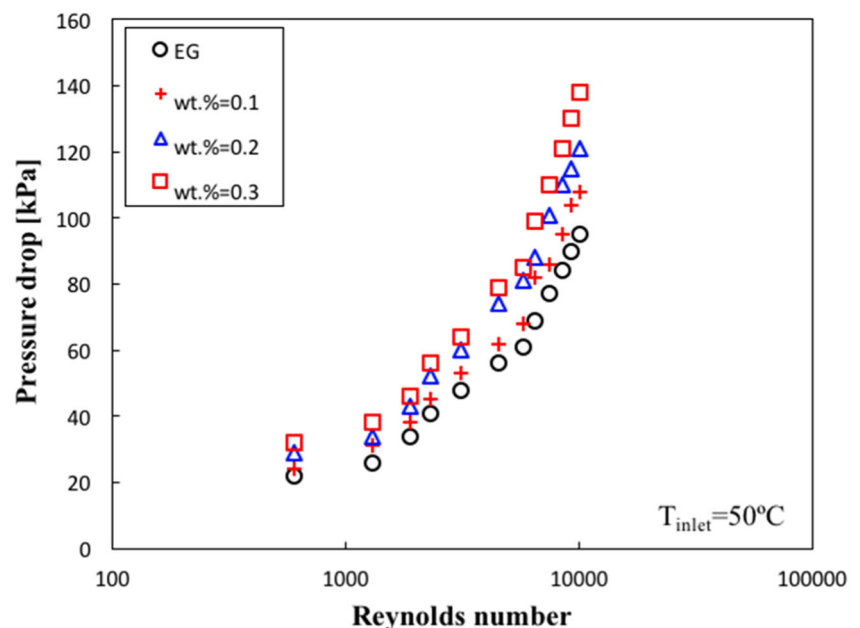
3.3 Inlet temperature

Figure 7 shows the dependence of the heat transfer coefficient on the Reynolds number for different inlet temperatures of the nanofluid to the heat exchanger. As can be

seen, with an increase in the inlet temperature of the nanofluid, the heat transfer coefficient slightly increases. For example, for a given Reynolds number such as $Re = 5800$, $wt.\% = 0.2$ and at $T = 40$ °C, the heat transfer coefficient is $4629 \text{ W/m}^2 \cdot \text{K}$, while it is $4699 \text{ W/m}^2 \cdot \text{K}$ at $T = 60$ °C. This is due to the small increment in the thermo-physical properties of the nanofluid such as thermal conductivity, density and viscosity of nanofluid. Notably, the thermal conductivity of the nanofluid increases slightly with an increase in the temperature. This is because due to the increase in temperature, Brownian motion together with the level of energy in nanoparticles increases resulting in better heat transfer within the base fluid. Noticeably, the heat transfer coefficient for the nanofluid at $wt.\% = 0.3$ was enhanced by 5.1, 7.2 and 9% at 40, 50 and 60 °C. Table 1 shows the result of enhancement in heat transfer coefficient and thermal conductivity for other mass concentrations of nanofluids.

Notably, Table 1 represents the obtained heat transfer coefficient (HTC) at various inlet temperatures of the heat exchanger at $Re = 4500$. As can be seen from Fig. 4, the influence of temperature on thermo-physical properties within the range of 25–60 °C is insignificant. Hence, with an increase in the inlet temperature of the working fluid, the HTC does not change significantly. Importantly, the uncertainty of the experiments for the HTC is ~9% and as can be seen, for the concentrations of 0.1 and 0.2%, the HTC enhancement is lower than the uncertainty, however, for $wt.\% = 0.3$, the enhancement is larger than uncertainty. Therefore, for the present work, the enhancement of HTC with inlet temperature at higher concentrations of nanoparticles is more reliable than lower mass concentration of nanoparticles.

Fig. 8 Dependence of pressure drop on Reynolds number for different nanofluids and the base fluid



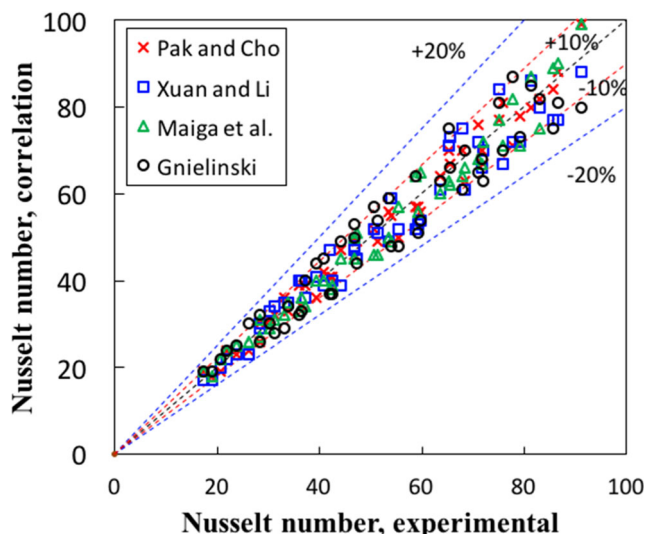


Fig. 9 Comparison between the experimental Nusselt number and those of estimated with the well-known correlations

3.4 Pressure drop and friction factor

Figure 8 presents the dependence of pressure drop on the Reynolds number for different nanofluids and for inlet temperature of 50 °C. As can be seen, with an increase in the flow fluid rate (Reynolds number), higher pressure drop was seen within the test section. Interestingly, with an increase in the mass concentration of the nanofluid, the pressure drop of the system increased. For example, at $Re = 7500$, at $wt.\% = 0.1$, pressure drop is 86 kPa, while for $wt.\% = 0.2$ and 0.3 , values of pressure drop are 101 kPa and 110 kPa, respectively. The maximum enhancement in pressure drop was $\sim 35\%$ at $wt.\% = 0.3$ and for the maximum $Re = 10,100$. Noticeably, the value

for the pressure drop of the base fluid was relatively lower than those of measured for the nanofluids. Importantly, the inlet temperature was found to have insignificant influence on the values of the pressure drop. These findings are in accordance with the results published in the literature [26] and the results presented in Fig. 4. The enhancement in the pressure drop can be attributed to the increase in the viscosity of the base fluid due to the presence of MgO nanoparticles. Interestingly, temperature did not change the viscosity significantly, thereby the inlet temperature did not have any remarkable influence on the pressure drop.

Figure 9 represents the results of a comparison between the experimental data and those of obtained with the well-known correlations namely Pak and Cho [27], Xuan and Li [28], Maiga et al. [29] and Gnielinski [30] correlations. Results of comparisons showed that the experimental Nusselt number is within the deviation of within ± 10.1 , ± 12.2 , ± 10.8 and $\pm 15.9\%$ against Pak and Cho, Xuan and Li, Maiga et al. and Gnielinski correlations. The deviation for the Glniski correlation is the highest because this correlation has been developed based on the experimental data obtained for the pure liquids. However, the other correlations have been developed for other nanofluids such as copper oxide/water, alumina/water and silica/water nanofluids. Hence, they are more accurate in predicting the Nusselt number. Overall, the obtained results in the present work is in accordance with the data published in the literature.

Figure 10 presents the dependence of friction factor on the Reynolds number for the nanofluids and also the base fluid. As can be seen, with an increase in the Reynolds number, the value for the friction factor decreases. However, for the mass concentration parameter, with an increase in the mass

Fig. 10 Dependence of friction factor on Reynolds number for different nanofluids and the base fluid

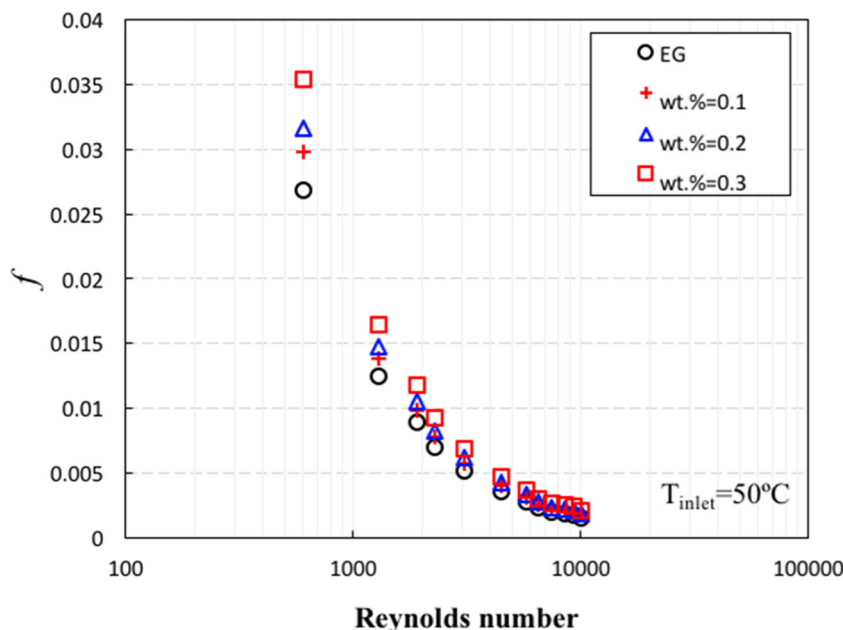
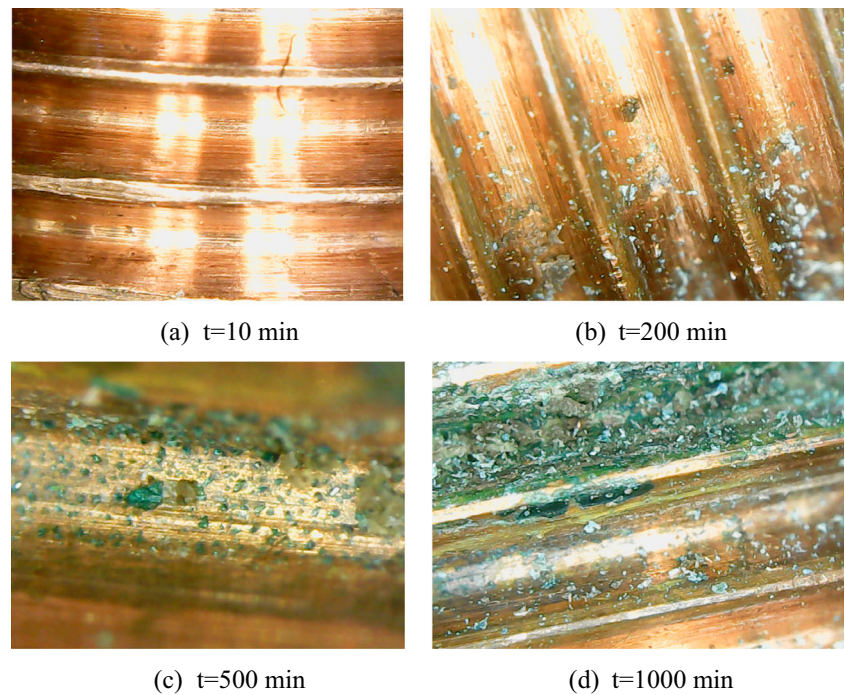


Fig. 11 The microscopy images taken from the internal surface of the heat exchanger where nanofluid passes through it to be cooled at different operating time



concentration of nanofluid, the friction factor slightly increases. The maximum augmentation in friction factor was 19% and for the $\text{wt.}\% = 0.3$. This is because, the increase in the number of nanoparticles within the base fluid increases the collision of nanoparticles with the walls of tube in the heat exchanger. This not only increases the friction forces between fluid and wall, but also increases the potential fouling on the walls of the heat exchanger. Fouling together with friction forces decrease the pressure along with the length of the heat exchanger. Noticeably, the friction factor for nanofluid, regardless of the concentration of nanoparticles, was higher than that of registered for the base fluid.

3.5 Fouling formation of nanoparticles within the heat exchanger

Figure 11 presents the results of a visualization study on the walls of the heat exchanger after 1000 min of the operation using a 200 x digital microscope manufactured by RS components. As can be seen, in the first 200 min of operation, there are some nanoparticles deposited on the internal wall of the heat exchanger, which is largely due to the gravitational forces, wall-particle attraction forces and particulate fouling of nanoparticles on the internal surface of the heat exchanger. With an increase in the time of operation, more nanoparticles are deposited on the surface (see Fig. 10c). According to the literature, fouling layer not only causes more pressure drop over the extended time, but also can increase the thermal fouling resistance, which decreases the heat transfer coefficient. Noticeably, in the present investigation, the nanoparticles did not create a continual layer

of the fouling. Hence, the thermal resistance between the surface and the bulk of the nanofluid did not appear. Also, the thickness of the fouling was very insignificant which had no influence on the pressure drop. The visualisation study also revealed that the higher, the number of nanoparticles, the probability of the fouling formation, the higher. Parameters such as flow rate, temperature of nanofluid, size of nanoparticles, stability of nanofluid and the type of the nanoparticles are potential parameters that can influence the particulate fouling rate inside the heat exchanger. These all need further investigations. For MgO/EG nanofluid, the fouling did not show any adverse effect on the thermal performance and heat transfer characteristics of the heat exchanger. Also, the indicative images provided in Fig. 11 show the importance of the particulate fouling in the heat exchanger body. Overall, a transient study on fouling over a long operation of the heat exchanger is highly recommend which is currently undergone and is beyond the scope of the present investigation. Notably, in the present investigation, fouling was investigated for a period of 1000 min and longer operation might reveal some interesting phenomena and new characteristics of the fouling formation of the MgO nanoparticles [31–36].

4 Conclusion

In the present work, an experimental investigation on the plausible application of MgO-ethylene glycol nanofluid in a double pipe heat exchanger was conducted and following conclusions were drawn:

- (1) Results showed that the presence of MgO nanoparticles within the ethylene glycol enhances the thermal conductivity and viscosity of nanofluid, while it decreases the heat capacity of the nanofluid. Within the temperature range of 25–60 °C, the maximum enhancement for the thermal conductivity and viscosity of the nanofluid were 55.4 and ~5% at wt.% = 0.3, while the highest reduction in the heat capacity was 1.5% at wt.% = 0.3
- (2) The presence of nanoparticles within the base fluid increased the pressure drop inside the heat exchanger. This was attributed to the enhancement in the viscosity of the ethylene glycol due to the presence of the nanoparticles. The maximum augmentation in the pressure drop was 35% and for wt.% = 0.3. For the friction factor, the same trend was seen and the maximum augmentation for the friction factor was 19% at wt.% = 0.3.
- (3) The inlet temperature slightly increased the heat transfer coefficient up to 9% at 60 °C. The reason for the enhancement was attributed to the increase in some thermo-physical properties such as thermal conductivity of nanofluid.

Overall, MgO-ethylene glycol can be a promising option for the heat transfer applications, however, slight pressure drop and friction factor augmentation together with a very small amount of particulate fouling are downside of the application of this nanofluid in the heat exchanging systems, which need to be addressed properly. In the present study, the thermal performance of MgO-EG nanofluid for 1000 min of operation was successful.

Acknowledgments Authors of this work tend to appreciate Bandar Abbas University for their facilities. Also, one author of this work appreciates the Elite and young researcher club for their financial supports.

Compliance with ethical standards

Conflict of interest On behalf of other authors of this manuscript, the corresponding author declares that there is no conflict of interest in this paper. All financial resources were also acknowledged.

Publisher's note Springer Nature remains neutral with regard to jurisdictional claims in published maps and institutional affiliations.

References

1. Kakac S, Liu H, Pramuanjaroenkij A (2012) Heat exchangers: selection, rating, and thermal design. CRC press, Boca Raton
2. T'Joel C, Park Y, Wang Q, Sommers A, Han X, Jacobi A (2009) A review on polymer heat exchangers for HVAC&R applications. *Int J Refrig* 32:763–779
3. Sundén B, Manglik RM (2007) Plate heat exchangers: design, applications and performance. Wit Press, Southampton
4. Focke W, Zachariades J, Olivier I (1985) The effect of the corrugation inclination angle on the thermohydraulic performance of plate heat exchangers. *Int J Heat Mass Transf* 28:1469–1479
5. Grijpspeerdt K, Hazarika B, Vucinic D (2003) Application of computational fluid dynamics to model the hydrodynamics of plate heat exchangers for milk processing. *J Food Eng* 57:237–242
6. Eastman JA, Choi S, Li S, Yu W, Thompson L (2001) Anomalous increased effective thermal conductivities of ethylene glycol-based nanofluids containing copper nanoparticles. *Appl Phys Lett* 78:718–720
7. Han D, He W, Asif F (2017) Experimental study of heat transfer enhancement using nanofluid in double tube heat exchanger. *Energy Procedia* 142:2547–2553
8. Bahiraei M, Godini A, Shahsavari A (2018) Thermal and hydraulic characteristics of a minichannel heat exchanger operated with a non-Newtonian hybrid nanofluid. *J Taiwan Inst Chem Eng* 84: 149–161
9. Kabeel A, El Maaty TA, El Samadony Y (2013) The effect of using nano-particles on corrugated plate heat exchanger performance. *Appl Therm Eng* 52:221–229
10. Bhattad A, Sarkar J, Ghosh P (2018) Discrete phase numerical model and experimental study of hybrid nanofluid heat transfer and pressure drop in plate heat exchanger. *Int Commun Heat Mass* 91:262–273
11. Tiwari AK, Ghosh P, Sarkar J (2013) Heat transfer and pressure drop characteristics of CeO₂/water nanofluid in plate heat exchanger. *Appl Therm Eng* 57:24–32
12. Bashirmezhad K, Ghavami M, Alrashed AA (2017) Experimental investigations of nanofluids convective heat transfer in different flow regimes: a review. *J Mol Liq* 244:309–321
13. Naik BAK, Vinod AV (2018) Heat transfer enhancement using non-Newtonian nanofluids in a shell and helical coil heat exchanger. *Exp Thermal Fluid Sci* 90:132–142
14. Kumar V, Tiwari AK, Ghosh SK (2017) Characterization and performance of nanofluids in plate heat exchanger. *Mater Today: Proceedings* 4:4070–4078
15. Zhang C, Zhang L, Xu H, Wang D, Ye B (2017) Investigation of flow boiling performance and the resulting surface deposition of graphene oxide nanofluid in microchannels. *Exp Thermal Fluid Sci* 86:1–10
16. Das SK, Putra N, Roetzel W (2003) Pool boiling characteristics of nano-fluids. *Int J Heat Mass Transf* 46:851–862
17. Anoop K, Cox J, Sadr R (2013) Thermal evaluation of nanofluids in heat exchangers. *Int Commun Heat Mass* 49:5–9
18. Sarafraz MM, Hormozi F (2014) Forced convective and nucleate flow boiling heat transfer to alumina nanofluids. *Period Polytech Chem Eng* 58:37–46
19. Sarafraz M, Hormozi F, Kamalgharibi M (2014) Sedimentation and convective boiling heat transfer of CuO-water/ethylene glycol nanofluids. *Heat Mass Transf* 50:1237–1249
20. Sarafraz MM, Hormozi F, Silakhori M, Peyghambarzadeh SM (2016) On the fouling formation of functionalized and non-functionalized carbon nanotube nano-fluids under pool boiling condition. *Appl Therm Eng* 95:433–444
21. Nakhjavani M, Nikkhah V, Sarafraz MM, Shoja S, Sarafraz M (2017) Green synthesis of silver nanoparticles using green tea leaves: Experimental study on the morphological, rheological and antibacterial behaviour. *Heat Mass Transf* 53:3201–3209
22. Adams T, Dowling M, Abdel-Khalik S, Jeter S (1999) Applicability of traditional turbulent single-phase forced convection correlations to non-circular microchannels. *Int J Heat Mass Transf* 42:4411–4415
23. Qi S, Zhang P, Wang R, Xu L (2007) Single-phase pressure drop and heat transfer characteristics of turbulent liquid nitrogen flow in micro-tubes. *Int J Heat Mass Transf* 50:1993–2001

24. Williams W, Buongiorno J, Hu L-W (2008) Experimental investigation of turbulent convective heat transfer and pressure loss of alumina/water and zirconia/water nanoparticle colloids (nanofluids) in horizontal tubes. *J Heat Transf* 130:042412
25. Sarafraz MM, Nikkiah V, Madani SA, Jafarian M, Hormozi F (2017) Low-frequency vibration for fouling mitigation and intensification of thermal performance of a plate heat exchanger working with CuO/water nanofluid. *Appl Therm Eng* 121:388–399
26. Duangthongsuk W, Wongwises S (2010) An experimental study on the heat transfer performance and pressure drop of TiO₂-water nanofluids flowing under a turbulent flow regime. *Int J Heat Mass Transf* 53:334–344
27. Pak BC, Cho YI (1998) Hydrodynamic and heat transfer study of dispersed fluids with submicron metallic oxide particles. *Exp Heat Transfer* 11:151–170
28. Xuan Y, Li Q (2003) Investigation on convective heat transfer and flow features of nanofluids. *J Heat Transf* 125:151–155
29. El Bécaye Maïga S, Tam Nguyen C, Galanis N, Roy G, Maré T, Coqueux M (2006) Heat transfer enhancement in turbulent tube flow using Al₂O₃ nanoparticle suspension. *Int J Numer Method H* 16:275–292
30. Bergman TL, Incropera FP, DeWitt DP, Lavine AS (2011) *Fundamentals of heat and mass transfer*. Wiley, New York
31. Tabassum R, Mehmood R, Pourmehran O, Akbar NS, Gorji-Bandpy M (2018) Impact of viscosity variation on oblique flow of Cu–H₂O nanofluid. *Proceedings of the Institution of Mechanical Engineers, Part E: Journal of Process Mechanical Engineering* 232:622–631
32. Yousefi M, Pourmehran O, Gorji-Bandpy M, Inthavong K, Yeo L, Tu J (2017) CFD simulation of aerosol delivery to a human lung via surface acoustic wave nebulization. *Biomech Model Mechanobiol* 16:2035–2050
33. Pourmehran O, Rahimi-Gorji M, Gorji-Bandpy M, Baou M (2015) Comparison between the volumetric flow rate and pressure distribution for different kinds of sliding thrust bearing. *Propulsion and Power Research* 4:84–90
34. Sarafraz MM (2013) Experimental investigation on pool boiling heat transfer to formic acid, propanol and 2-butanol pure liquids under the atmospheric pressure. *J Appl Fluid Mech* 6:73–79
35. Sarafraz MM, Hormozi F, Peyghambarzadeh SM, Vaeli N (2015) Upward flow boiling to DI-water and CuO nanofluids inside the concentric annuli. *Appl Fluid Mech* 8:651–659
36. Nikkiah V, Sarafraz MM, Hormozi F (2015) Application of spherical copper oxide (II) water nano-fluid as a potential coolant in a boiling annular heat exchanger. *Chem Biochem Eng Q* 29:405–415